

Rapid Microwave-Assisted Ionothermal Dissolution of Cellulose and Its Regeneration Properties

Xu Wang^{1,3}, Jianhong Zhou^{1,2}, Bo Pang^{1,2} and Dawei Zhao^{1,2,*}

¹Key Laboratory on Resources Chemicals and Materials of Ministry of Education, Shenyang University of Chemical Technology, Shenyang, 110142, China.

²Institute of Industrial Chemistry and Energy Technology, Shenyang University of Chemical Technology, Shenyang, 110142, China.

³College of Environmental and Safety Engineering, Shenyang University of Chemical Technology, Shenyang, 110142, China.

*Corresponding Author: Dawei Zhao. Email: syzhaodawei2014@nefu.edu.cn.

Abstract: Introduction of the strategy of anhydrous calcium carbonate protection incorporated with the drop by drop reaction, high-purity 1-butyl-3-methylimidazolium chloride ([Bmim] Cl) was prepared at reaction temperature of 80°C for only 10 h. Cellulose samples from different biomass sources (with different degree of polymerization characteristic) could be rapidly (no more than 10 minutes) and completely dissolved in the [Bmim] Cl using a microwave-assisted ionothermal route. Homogeneous cellulosic regenerates with high degree of polymerization and thermal stability characteristics were obtained through a coagulation process in water. Furthermore, the dissolved celluloses were readily regenerated into solid products such as casting films and spinning fibers, which exhibited high transparency and flexibility, as well as superior mechanical properties of over 300 MPa (tensile strength) more than those of cellulose samples reported. This study therefore provides a new process for the synthesis of high-purity [Bmim] Cl for the highly efficient dissolution of cellulose to produce high performance cellulosic materials for various applications such as flexible electronic, optoelectronic, soft robots.

Keywords: Ionic liquid; cellulose; ionothermal; transparent film

1 Introduction

Cellulose is the most abundant organic compound found on earth and has several attractive properties, including biocompatibility, biodegradability and good chemical and thermal stabilities. Cellulose has also become an important source of raw materials in the biorefinery and materials industries [1-5]. Cellulose consists of a linear chain of β -1, 4-linked D-glucose units, with a large number of inter- and intra-molecular hydrogen bonds between the individual polymeric chains, leading to its poor solubility in water and most organic solvents [6]. Several solvent systems, including N-methylmorpholine-N-oxide (NMMO), dimethyl sulfoxide/tetrabutylammonium fluoride (DMSO/TBAF), N, N-dimethyl acetamide/lithium chloride (DMAc/LiCl), lithium perchlorate trihydrate (LiClO₄·3H₂O) and NaOH/urea aqueous solution have been developed for the dissolution of cellulose [7-11]. However, the application of these solvent systems has been limited by their poor stability, toxicity, high cost, harsh processing conditions and difficulties associated with their recovery. There is therefore an urgent need for the development of environmentally friendly and highly efficient solvent systems to minimize contamination and reduce the costs associated with processes involving the dissolution of cellulose.

The discovery of a specific group of ionic liquids (ILs), known as 1, 3-dialkylimidazolium chlorides, led to the development of ILs as a new class of cellulose solvents, which have subsequently been used to produce a wide range of cellulosic materials *via* various reconstitution processes [6]. Compared with traditional solvents, ILs exhibit several unique properties, including wide liquidus regions, high thermal stabilities and negligible vapor pressures. Furthermore, ILs do not give rise to any toxic or explosive gases during their treatment processes, making them “green” solvents [12]. The combination of anions and cations used in an IL has a pronounced effect on its physical and chemical properties, including its melting point, viscosity, hydrophobicity and stability towards hydrolysis. Increasing the basicity of the anions whilst decreasing the hydrogen bond donor capability of the cations afford ILs with a pronounced ability to dissolve cellulose. A high-throughput screening result showed that halide-containing imidazolium-based ILs are among the most effective ILs for dissolving (ligno-) celluloses, with 1-butyl-3-methylimidazolium chloride ([Bmim] Cl) being one of the most commonly reported examples from this class of ILs [13,14]. The synthesis of [Bmim] Cl has been studied extensively and the most commonly used method for the synthesis of this IL is the “one-step” mixing of N-methylimidazole with n-butyl chloride under an atmosphere of nitrogen and in organic solvent over an extended period (e.g., 48-72 h). Although the results of several previous studies pertaining to the synthesis of [Bmim] Cl have revealed several important findings (e.g., non-toxic, chemical stability and retrievability), further research towards decreasing the energy consumption of the [Bmim] Cl preparation process and improving the efficiency of this solvent for the dissolution of cellulose is still needed.

The purity of an IL plays an important role in determining its physicochemical qualities and practical applications [15]. In contrast to conventional ionothermal methods, microwave heating has been shown to be a faster and greener approach, producing high yields and good phase purities for the construction of specific targets [16]. In this study, we have designed a novel method, using anhydrous calcium carbonate protection combined with “drop by drop reaction”, for the synthesis of high-purity ILs by controlling the effective collision between n-butyl chloride and N-methylimidazole. The resulting [Bmim] Cl material led to considerable improvements in the dissolution efficiencies of cellulose samples from wood, catkin and linter using a microwave-enhanced ionothermal process. These cellulose/IL solutions were subsequently used to prepare cellulosic films (by casting) and fibers (by spinning) after the phase conversion process. The properties of these materials, including their transparency, structure, micromorphology, thermal properties and mechanical strength were fully characterized using standard techniques.

2 Materials and Methods

2.1 Materials

Three biomass sources, including poplar wood (*Populus ussuriensis*), catkin (*Salix matsudana*) and linter (purchased from the China National Cotton Group Corp., Beijing, China), were ground and sieved (60 mesh) to give fine powders. The cellulose in these powders was subsequently extracted using a previously reported method [4]. The chemical compositions of the resulting cellulose extracts are listed in Tab. S1. N-Methylimidazole ($C_4H_6N_2$), n-butyl chloride (C_4H_9Cl), silver nitrate and anhydrous calcium carbonate were purchased from Aladdin Chemistry Co., Ltd. (Shanghai, China). Acetone and diethyl ether were purchased from Kermel Chemical Reagent Co., Ltd (Tianjin, China). Copper ammonia solution was purchased from Aaron biotechnology Co., Ltd (Tianjin, China). All of the chemicals used in this study were purchased as the analytical grade and without further purification.

2.2 Synthesis of [Bmim] Cl

The 79.72 ml of freshly distilled N-methylimidazole (1 mol) was placed in a 500-ml three-necked flask equipped with a condenser, the top of which was fitted with a drying tube filled with anhydrous calcium carbonate to remove moisture and isolate oxygen during the air circulation process. The

three-necked flask was heated at 60°C in an oil bath for 5 min. A 92.57 g of n-butyl chloride (1.05 mol) was then added to the three-necked flask in a dropwise manner at 60°C, stirring at 2000 rpm, using a dropping funnel to improve the effective collision of reactants and shorten reaction time, and the resulting mixture was heated at under reflux at 80°C with stirring at 1500 rpm for 10 h. The mixture when cooled to 40°C was poured into 200 mL of a 2:3 (v/v) mixture of acetone and diethyl ether (ADE). The resulting mixture was stirred using glass bar for 10 min to ample dissolve the remaining reactants in (ADE), and the crystal of [Bmim] Cl was growing up as the mixture was cooled to room temperature. The white crystals of [Bmim] Cl obtained were dried under vacuum at 80°C for 4 h to remove the volatile impurities, leading to a viscous, colorless and transparent liquid product.

2.3 Dissolution of Cellulose under Microwave-Solvothermal Conditions

Four samples (0.242, 0.364, 0.488 and 0.612 g) of the celluloses collected from wood, catkin and linter were added to 30 g of [Bmim] Cl (preparing the 0.8, 1.2, 1.6 and 2.0 wt% cellulose/IL, respectively) under vigorous stirring. The resulting mixtures were heated in a WM-2 microwave muffle furnace (PreeKem Instrument Co. Ltd, Shanghai, China) at 80°C and 1000 W. The extent to which each cellulose sample dissolved in [Bmim] Cl was measured on a minute-by-minute basis using a microscope (SZ61/SZ51, Changfang Optics Co. Ltd., Shanghai, China), until a translucent solution was obtained.

2.4 Preparation of Cellulose Films

A cellulose/IL solution was placed in a vacuum oven under absolute pressure (0.01 MPa) at 90°C for 30 min to remove air bubbles. The solution was then cast on a silicon wafer with a diameter of 50 mm using a VTC-100 (Kejing Auto-instrument Co. Ltd, Shenyang, China). The silicon wafer was then taken out and immersed in distilled water at 60°C, where it was held for 4 h to give a hydrogel. The resulting hydrogel film was rinsed with distilled water until no white precipitates were generated during its titration against a 0.01 mol/L aqueous solution of silver nitrate. The hydrogel was then sandwiched between two silicon wafers and dried in a vacuum oven (0.05 MPa) at 60°C for 24 h to give a transparent and flexible dry film. The different thickness of films was obtained by controlling the coating speed and time of vacuum spin coater and pressure of the sandwich construction in the drying process.

2.5 Preparation of Cellulose Fibers

A cellulose/IL solution was transferred to a 5-mL plastic syringe (internal diameter of 0.7 mm) and degassed according to the procedure described above. Fibers were subsequently extruded from the syringe in the speed of 5 cm/min into a water bath at 35°C, where they were soaked at the same temperature for 60 min. The cellulose fibers were obtained after oven-dried at 60°C for 24 h.

2.6 Characterization

¹³C CP/MAS NMR analysis of the extracted cellulose was carried out on a BRUKER DRX-500 NMR spectrometer (Bruker Instruments, Rheinstetten, Germany). Spectra were acquired with a 4-mm magic angle sample spinning probe. A total of 800 scans were accumulated for each sample. ¹³C and ¹H NMR spectra of the IL and cellulose/IL solutions (8 wt%, 0.2 g) in DMSO-d₆ (2 mL) were collected on a BRUKER DRX-500 NMR spectrometer. These spectra were collected at 27°C with 20,000 scans per sample at 125.75 MHz. Chemical shifts were given in ppm downfield from tetramethylsilane, which was used as an internal reference. The relaxation times were set at 2 and 1 s for the ¹³C and ¹H NMR, respectively. The Fourier transform infrared (FTIR) spectra of the IL and the regenerated cellulose materials prepared in the current study were measured using a Nicolet 6700 FTIR instrument (Thermo Fisher Scientific Inc., Waltham, MA, USA). All of the spectra were measured in the ATR mode, with data recorded in the range of 650-4000 cm⁻¹ over 32 scans with a resolution of 4 cm⁻¹. The viscosity of the IL and the cellulose/IL solutions was measured at different temperature conditions using an NDJ-5S

digital viscosimeter (Weide Instrument Co., Ltd, Yuyao, China), with five tests being performed for each sample. The α -cellulose contents of the extracted and regenerated cellulose samples were determined as previously described [4]. At least five tests were conducted for each sample, and the average was calculated. A sample (2 g) of a cellulose/IL solution (cellulose content 0.8 wt%) was added to 50 mL of distilled water. Uniform suspension was obtained under ultrasonic irradiation at 30 kHz for 30 min in an ultrasonic cleaner (Law Rand Ultrasonic Technology Co., Ltd., Hangzhou, China). A self-designed columnar filtration unit filled with quartz granules (Fig. S2) was used to wash the regenerated cellulose. The resulting gel product was then added to 50 mL of distilled water and oscillated under ultrasonic irradiation at 30 kHz for 45 min. A droplet (5 μ L) of the diluted slurry was then dropped onto a carbon-coated electron microscopy grid, which was subjected to transmission electron microscopy (TEM) observation using a FEI Tecnai G2 microscope at an acceleration voltage of 80 kV. X-ray diffraction (XRD) of the regenerated cellulose were obtained using a D/max 2200 X-ray diffractometer (Rigaku, Tokyo, Japan) equipped with Ni-filtered Cu-K α radiation ($\lambda = 0.154$ nm). The samples were scanned within 5-30° 2θ at 40 kV and 30 mA with a scanning rate of 4° min $^{-1}$. Thermogravimetric (TG) analysis of the regenerated cellulose was performed using a STA 6000 TG analyzer (Perkin Elmer Inc., Waltham, MA, USA) at temperatures in the range of 40-850°C at a heating rate of 20°C min $^{-1}$ under a nitrogen atmosphere (40 mL min $^{-1}$). The light transmittance properties of the regenerated cellulose films were measured using a TU-1901 spectrophotometer (Purkinje General Instrument Co., Ltd., Beijing, China) for wavelengths in the range of 400-800 nm. The micromorphological characteristics of the regenerated cellulose materials were observed using a field emission scanning electron microscope (SEM, JSM-7500F, Hitachi, Tokyo, Japan) at an acceleration voltage of 10 kV. The morphological and roughness characteristics of the surfaces of the cellulose films were observed using an atomic force microscopy (AFM, Multimode 8 AFM microscope (Bruker) in the peak force tapping mode. The Nanoscope V7.30 software was applied to analyze the data. Tensile properties of the cellulose films and fibers were measured on an Instron 5569 universal testing machine at room temperature with a cross-head speed of 1 mm min $^{-1}$. The sizes of the films for testing were 15 \times 5 \times (0.02-0.05) mm (length/width/thickness). The sizes of the fibers for testing were 15 \times (0.01-0.04) mm (length/diameter). The thickness values of the films and fibers are obtained using Micron micrometer with 0.001 mm accuracy (Shanghai Songxin measuring instruments factory, China).

2.7 Degree of Polymerization

Degree of polymerization (DP). The DP of cellulose (both extracted and regenerated) was measured and calculated using the Ubbelohde viscometer (1835-4-0.80, Xinbiao Tengda Instrument Equipment Co., Ltd., Beijing, China) according to the following equations:

$$(\text{DP}) = \frac{\eta}{0.0005 \times C(1 + 0.29\eta)} \quad (1)$$

where η is the specific viscosity and C is the mass concentration (g L $^{-1}$) of the cellulose/copper ammonia solution.

$$\eta = \frac{t - t_0}{t_0} \quad (2)$$

where t is the outflow time of the cellulose/copper ammonia solution (s) and t_0 is the outflow time of a 0.5- mol L $^{-1}$ standard copper ammonia solution (s).

3 Results and Discussion

3.1 Characterization of the Synthesized IL

We skillfully placed a drying tube filled with anhydrous calcium carbonate on top of the condensing tube. Due to the strong hygroscopicity and oxygen barrier of anhydrous calcium carbonate, the obtained [Bmim] Cl exhibits a colorless and transparent behavior, which indicates the [Bmim] Cl is

of good purity (Fig. S1). More importantly, due to the high efficiency collisions in the drop by drop reaction process, it takes only 10 h to make the yield of the [Bmim] Cl exceed 90%, which is superior to that of common method-one-time addition of n-butyl chloride into N-methylimidazole (Fig. S2). The structure of the [Bmim] Cl prepared in this study was characterized by FTIR and NMR spectroscopy. The FTIR spectrum (Fig. 1(a)) contained several characteristic absorption peaks at 3066 cm^{-1} (C-H stretching vibration of the imidazole ring), 2870 and 2960 cm^{-1} (C-H stretching vibrations of pendant butyl and methyl groups, respectively), 1560 cm^{-1} (-CN stretching vibration), 1470 cm^{-1} (-C=C- stretching vibration of the imidazole ring) and 1170 and $740\text{-}790\text{ cm}^{-1}$ (in- and out-of-plane bending vibrations of the C-H bonds, respectively). All of the observed absorption peaks were identical to those previously reported for the [Bmim] Cl in the literature [17]. The IL prepared in the current study was found to be strongly hygroscopic because of its high polarity, and was consequently transformed from a solid to a liquid after being stored in an open container at room temperature for 2.5 h (Fig. 1(a)). This change in the physical form of the material was accompanied by the appearance of a stretching vibration at 3340 cm^{-1} , which was attributed to the -OH groups of water molecules adsorbed by this hygroscopic material [17]. The ^{13}C and ^1H NMR spectra (Fig. 1(b)) of the IL showed that it contained eight C atoms and fifteen H atoms. The chemical shifts of these signals (Tab. 1) were consistent with those previously reported for the [Bmim] Cl under similar conditions. These results therefore confirm that the structure of the [Bmim] Cl prepared in the current study is consistent with the proposed structure and that the chemical purity of this material is suitably high.

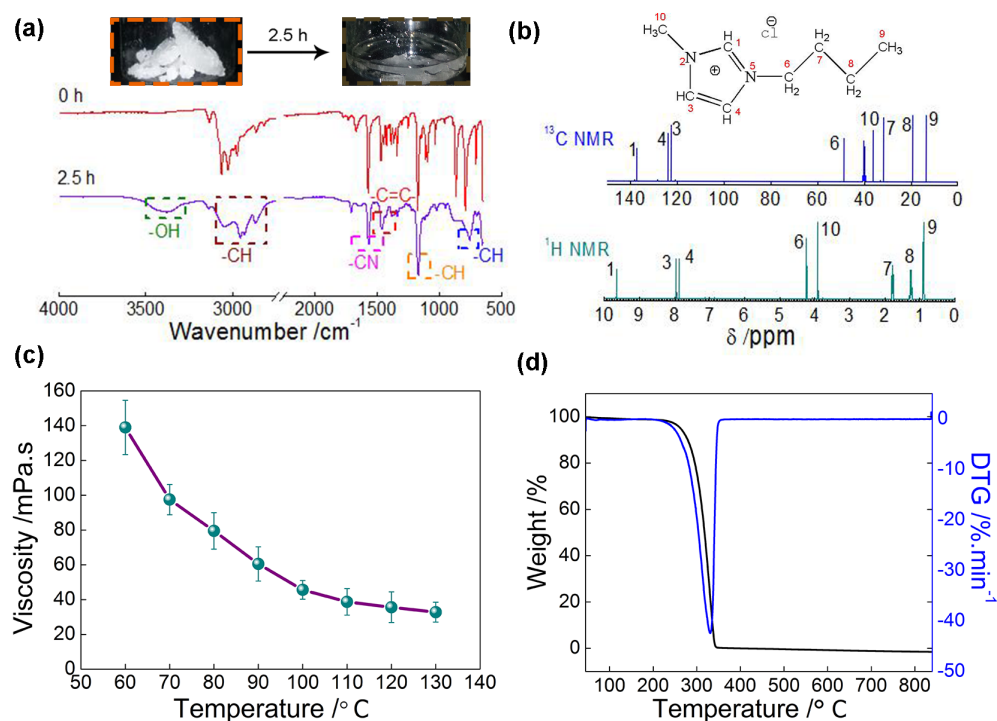
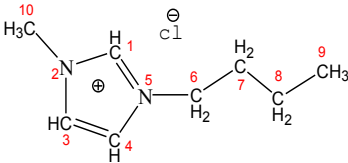


Figure 1: Properties of the [Bmim] Cl material prepared in this study. (a) FTIR spectra corresponding to solid (0 h) and hydration (after exposing in air for 2.5 h) states of the IL. The inset images in (a) are digital photographs of [Bmim] Cl before (left) and after (right) being exposed to air for 2.5 h; (b) $^{13}\text{C}/125\text{ MHz}$ and $^1\text{H}/500\text{ MHz}$ NMR spectra of the [Bmim] Cl; (c) Viscosity of the [Bmim] Cl as a function of temperature and its tendency towards crystallization under 60°C ; (d) TG and DTG curves of the [Bmim] Cl

Table 1: Chemical shifts of the C and H atoms in [Bmim] Cl

| Molecular formula | Chemical shifts (ppm) | | | | | | | |
|---|----------------------------|----------------------------|----------------------------|----------------------------|----------------------------|----------------------------|----------------------------|-----------------------------|
| | C ₁ | C ₃ | C ₄ | C ₆ | C ₇ | C ₈ | C ₉ | C ₁₀ |
|  | 137.5 | 122.6 | 124.0 | 48.50 | 32.85 | 19.26 | 13.56 | 36.08 |
| | H_{1-(s,1)} | H_{3-(s,1)} | H_{4-(s,1)} | H_{6-(t,2)} | H_{7-(m,2)} | H_{8-(m,2)} | H_{9-(t,3)} | H_{10-(s,3)} |
| | 9.65 | 7.86 | 7.96 | 4.25 | 1.28 | 1.26 | 0.91 | 3.91 |

H_{1-(s,n)}: H₁ denotes the position of H in the chemical formula; *s* denotes the number of overlapping peaks; and *n* denotes the number of H atoms under the same chemical environment.

The viscosity of the IL showed a negative correlation with the temperature (Fig. 1(c)). Increasing the temperature would lead to an increase in the kinetic energy of the molecules, which would make a decrease of the interaction energies between the [Bmim] Cl molecules. This is why the viscosity decreases with increasing temperature. The viscosity of the IL is less than 40 mPa.s when the temperature increased in 110°C. The results of the TG and the derivative of TG (DTG) analyses (Fig. 1(d)) revealed that the IL started to lose mass from 250°C (that is, the [Bmim] Cl obtained by our method has no mass loss until 250°C) and that it continued to do so up to 340°C, with almost no residue being left after the decomposition process. These phenomena highlight the high purity and thermal stability of the [Bmim] Cl prepared via the drop by drop reaction process (Fig. S2).

3.2 Cellulose Dissolution and Properties of the Cellulose/IL Solution

[Bmim] Cl ionic liquid can absorb and transfer microwave energy [18], and could therefore be used promote the dissolution of cellulose. When the temperature rises to the specified setting value such as 80°C, the cellulose/IL will undergo a stable thermostatic phase, that is, the dissolution process of cellulose (Figs. S3 and 4). The dissolution rate of cellulose in the [Bmim] Cl varied considerably depending on the source of the cellulose (Fig. 2(a)). This is most likely because of differences in degree of polymerization (DP) and crystallinity of the different cellulose samples (Fig. S5). For example, the cellulose sample from wood dissolved much more readily in the [Bmim] Cl than the cellulose samples from linter and catkin under the same conditions. More specifically, the linter cellulose, which had the most hydrogen bonds of the three cellulose samples evaluated in the current study, needed the longest time (10 min) to dissolve in the [Bmim] Cl. In contrast, the cellulose samples from catkin and wood required only 8 and 4 min, respectively, to reach complete dissolution. The maximum dissolution levels of the cellulose samples from wood (DP≈1484), catkin (DP≈1833) and linter (DP≈2265) in the [Bmim] Cl were 12.8, 8.4 and 6.8 wt%, with dissolution times of 18, 45 and 72 min, respectively (Fig. 2(b)). All of these solutions were transparent in appearance and exhibited the typical characteristics of a viscous solution. The viscosities of the cellulose/IL solutions decreased with increasing temperature up to a temperature of 90°C (Fig. 2(c)), at which point the viscosities of the solutions reached a plateau of less than 1500 mPa s (inset of Fig. 2(c)). Based on this result, we selected a temperature of 90°C as the optimum temperature for the coating membrane and spinning fiber experiments.

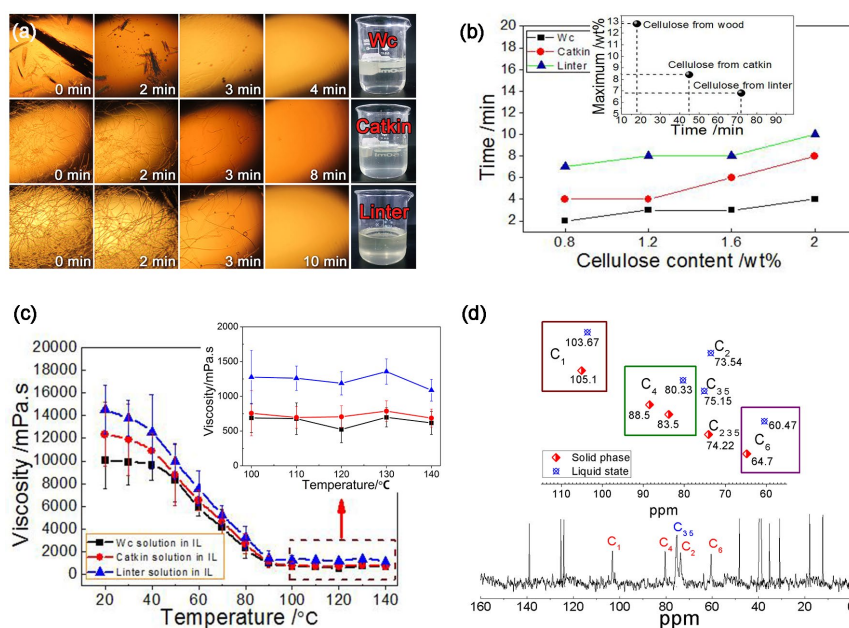


Figure 2: (a) Optical images showing the dissolving processes of the different cellulose samples taken from wood, catkin and linter in the [Bmim] Cl under microwave-assistant heating (cellulose content 2.0 wt%, heating temperature 80°C); (b) Comparison of the three different cellulose samples dissolved in the [Bmim] Cl. The inset panel shows a comparison of the maximum solute content and dissolution time; (c) Changes in viscosity of the cellulose/IL solution (2.0 wt% cellulose) with increasing temperature; (d) Comparison of the ^{13}C NMR spectra of the cellulose samples dissolved in the [Bmim] Cl with those of the original cellulose samples

A comparison of the ^{13}C NMR spectrum of the wood cellulose/IL solution with that of the original solid wood cellulose sample revealed considerable changes in the chemical shifts of five carbon peaks in the range of 55-110 ppm (Fig. S6). After dissolution, the C₄ peaks at 83.5 and 88.5 ppm in the crystalline region merged into one peak (80.33 ppm), whereas the C₂ peak (73.54 ppm) separated to form a C_{2,3,5} overlapped peak (74.22 ppm). These changes were attributed to the dispersion of the macromolecular chains of the cellulose sample in solution to form a dissociated state. The 0-55 and 110-160 ppm regions of the spectrum (Fig. 2(d), below) provide important information pertaining to the chemical shifts of the [Bmim] Cl. Compared with the pure [Bmim] Cl (Fig. 1(a)), the chemical shifts of the [Bmim] Cl in the cellulose/IL solution showed very few changes. We therefore concluded that the high solubility of cellulose in the [Bmim] Cl could be attributed to the formation of hydrogen bonding interactions between the hydroxyl protons of cellulose and the chloride anions and imidazolium cations of the [Bmim] Cl. These results therefore revealed that the dissolution of cellulose in the [Bmim] Cl is a physical process, and that this IL could be used as a non-derivatizing solvent for the dissolution of cellulose.

3.3 Properties of the Regenerated Cellulose Materials

Cellulose/IL solutions can be used to form various cellulosic materials, such as cellulose nanocrystals and cellulose-nanohydroxyapatite composites using coagulation processes. The process of cellulose reconstitution during coagulation in water (Fig. S7) was first observed using TEM. Ultrathin membranes with homogeneous and smooth surfaces were formed in the current study regardless of the cellulose sources (Figs. 3(a)-3(c)). Furthermore, these membranes could be folded without undergoing any fragmentation (Figs. 3(d) and 3(e)). The high-resolution electron diffraction patterns of these membranes showed circular diffraction tracks, which indicated that the membranes were mainly composed of amorphous phases, with partial crystalline phases (Fig. 3(f)).

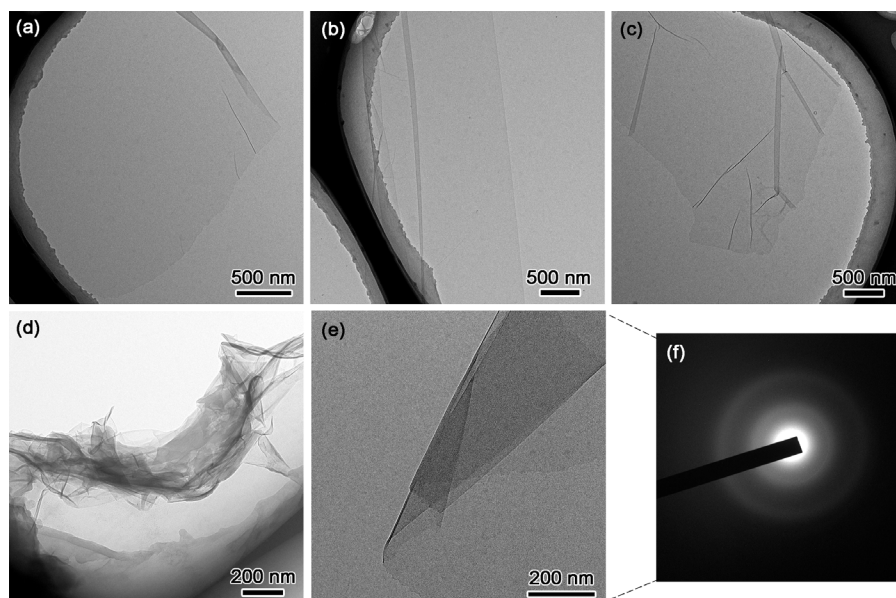


Figure 3: TEM images showing the microstructure of the regenerated cellulose samples taken from: (a) wood, (b) linter and (c) catkin; TEM images showing the (d) flexibility and (e) foldability of the ultrathin membranes; (f) High-resolution electron diffraction pattern showing the existence of the amorphous and crystalline phases of these cellulose materials

Changes in the functional groups of the cellulose samples after their dissolution and subsequent coagulation were revealed by FTIR analysis (Fig. 4(a)). The intensity of the absorption peak of the -OH bonds at 3360 cm^{-1} decreased after the dissolution process, most likely because of the weakening of the hydrogen bonding interactions between the individual cellulose molecules. The peaks in the range of $1000\text{-}1115\text{ cm}^{-1}$ also showed a decrease in their intensity for the same reason (i.e., -O-H...O hydrogen bonds). Furthermore, the -C=O stretching vibration of hemicellulose (1637 cm^{-1}) disappeared following the dissolution of the cellulose material in the [Bmim] Cl, indicating that the IL could be used to remove hemicellulose and therefore purify cellulose. The α -cellulose content of the regenerated product was determined to be 97% (Fig. 4(b), Tab. S1). The DP values of the different feedstocks were determined to be 2265, 1833 and 1484 for the linter, catkin and wood cellulose samples, whereas the values of the corresponding regenerated cellulose samples were approximately 20% lower (Fig. 4(c)). The molecular weights of the regenerated cellulose samples were estimated to be in the range of 220-300 kDa by multiplying their DP values by the molecular weight of an anhydroglucose unit (162). These values were therefore higher than those determined for cellulose using different methods [19,20]. And the DP of cellulose was progressively decreased with the temperature increasing (Fig. S8).

The XRD spectra of the original cellulose samples were collected together with those of the corresponding regenerated cellulose samples (Fig. 4(d)). The XRD spectra of the original cellulose samples contained diffraction peaks at 16.0° and 22.6° , which were attributed to cellulose I. In contrast, the regenerated materials contained cellulose II with lower crystallinity (Fig. S9), as exemplified by the appearance of smaller diffraction peaks in their XRD spectra at 12.2° and 21.9° . The regenerated cellulosic materials still have outstanding thermal stability over 300°C (Figs. 4(e) and 4(f)).

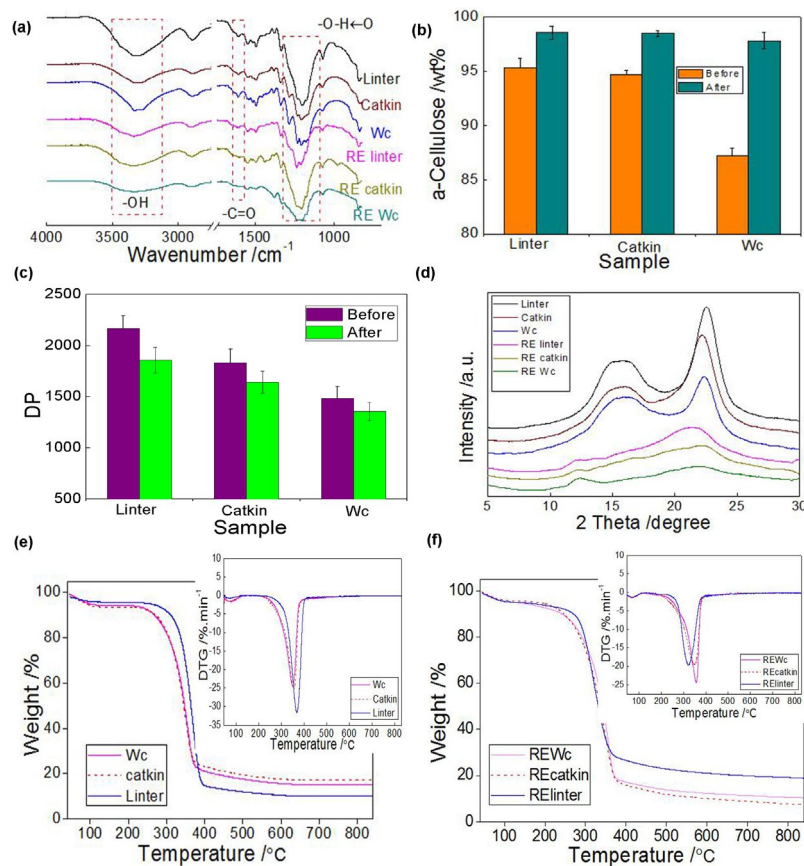


Figure 4: (a) FTIR spectra; (b) α -cellulose contents; (c) DP values; (d) XRD patterns and (e-f) TG and DTG curves of the original and regenerated cellulose samples

3.4 Preparation and Properties of Cellulose Films

A cellulose (2.0 wt%)/IL solution was cast onto a single-sided polished silicon slice on a vacuum spin coater to prepare practical cellulose films. After washing and vacuum drying, all of the films prepared in this way showed good transparency and flexibility (Fig. 5(a)). The films also exhibited light transmittance properties above 90% at 600 nm (Fig. 5(b)), which exceeded those of common plate glass (82%), glass paper (87%) [21] and acrylic resin (89%) [22]. Compared with the regenerated cellulose films from DMAc/LiCl and NaOH/urea solvents [22,23], our films showed equal or superior transmittance properties. The surfaces of our films appeared to be quite smooth and compact, with micropores and mesopores observed by SEM at high resolution (Figs. 5(c)-5(e)). The cellulose film of wood has more abundant pore structure than that of regenerated film from catkin or linter, which is more conducive to light transmission and reduce light scattering. AFM was used to study the nanoscale roughness of the films of wood, and the results revealed that the average roughness (R_a) and root-mean square roughness (R_q) values were both less than 12 nm. The maximum peak-to-valley differences were found to be 73.3, 78.4 and 85.2 nm for the regenerated cellulose films wood, catkin and linter, respectively (Fig. 5(g)). The other AFM pictures of the regenerated cellulose films were showed in Fig. S10.

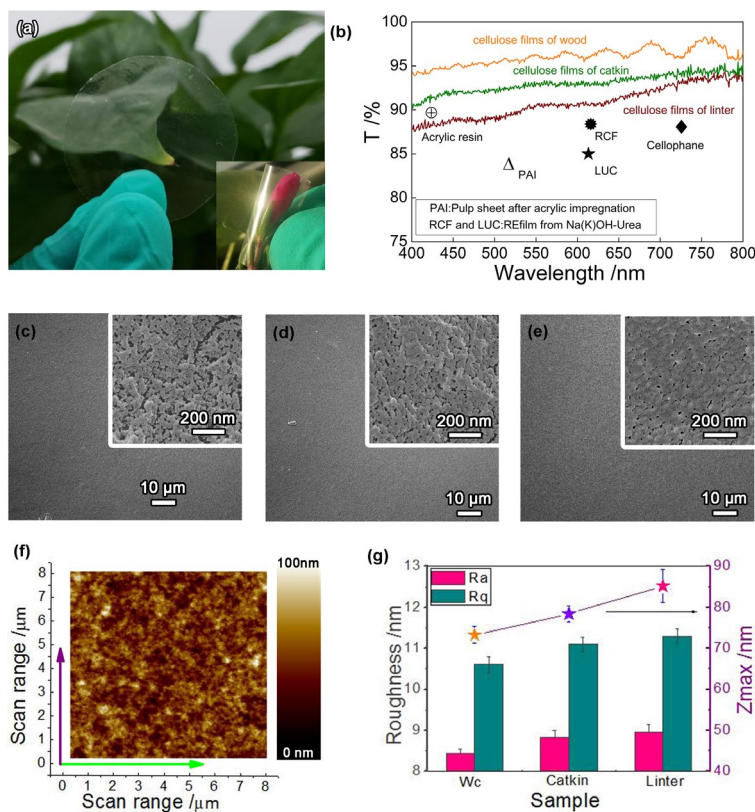


Figure 5: (a) Photographic images of the regenerated cellulose films from wood cellulose /IL solutions (2.0 wt%). Inset shows the excellent flexibility of the regenerated film; (b) The light transmittance properties of the regenerated films; (c-e) SEM images of the cellulose films of wood, catkin, and linter (from left to right); (f) Microtopography of the wood cellulose film observed by AFM and (g) profile roughness properties of the different cellulose films

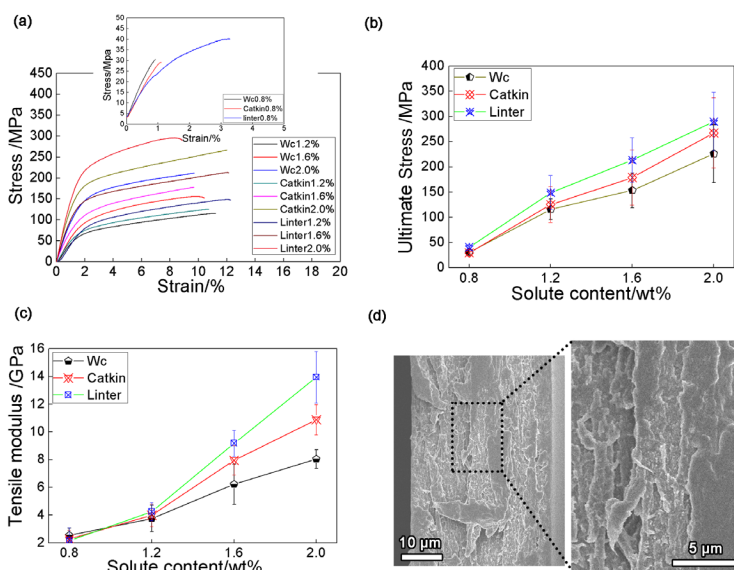


Figure 6: Mechanical properties of the cellulose films: (a) stress-strain curves; (b) ultimate tensile stress; (c) Young's modulus; and (d) SEM micrographs showing the fracture cross-section of a wood cellulose film

The stress-strain curves of the cellulose films prepared from cellulose/IL solutions with different cellulose sources and cellulose contents are shown in Fig. 6(a). When the cellulose content was as low as 0.8 wt%, the strength of the cellulose film was poor. Increasing the solute content from 0.8 to 2.0 wt% led to an increase in the ultimate tensile stress (UTS) from around 50 to 300 MPa (Fig. 6(b)). The UTS of the wood cellulose film (2.0 wt%) was greater than those of the cellulose films prepared from DMAC/LiCl solution [23], [Emim] Ac IL [24], NaOH/urea aqueous solution [25] and LiOH/urea aqueous solution [26]. The cellulose film regenerated from a 2.0 wt% linter cellulose/IL solution also gave a larger UTS than those made from bacterial cellulose [27], cellulose nanopaper [28] and nanofibrillated cellulose [29]. A similar trend was also observed in the Young's modulus values of these materials, which increased considerably with increasing cellulose content (Fig. 6(c)). The Young's modulus reached up to 14 GPa for a cellulose film prepared from a 2 wt% of linter cellulose/IL solution, which was greater than any of the values mentioned above for regenerated cellulose films [24-26] and cellulose nanopaper [28,29]. Furthermore, films prepared from cellulose/IL solutions with high solute contents exhibited interesting elastic-plastic behaviors (Fig. 6(a)). The fracture cross-sections of the films were quite different from their surfaces, in that they displayed isotropic and compact microstructures (Fig. 6(d)). These transparent, strong cellulosic films could potentially be used in a wide range of applications, including optics, electronics and materials science.

3.5 Preparation and Properties of Cellulose Fibers

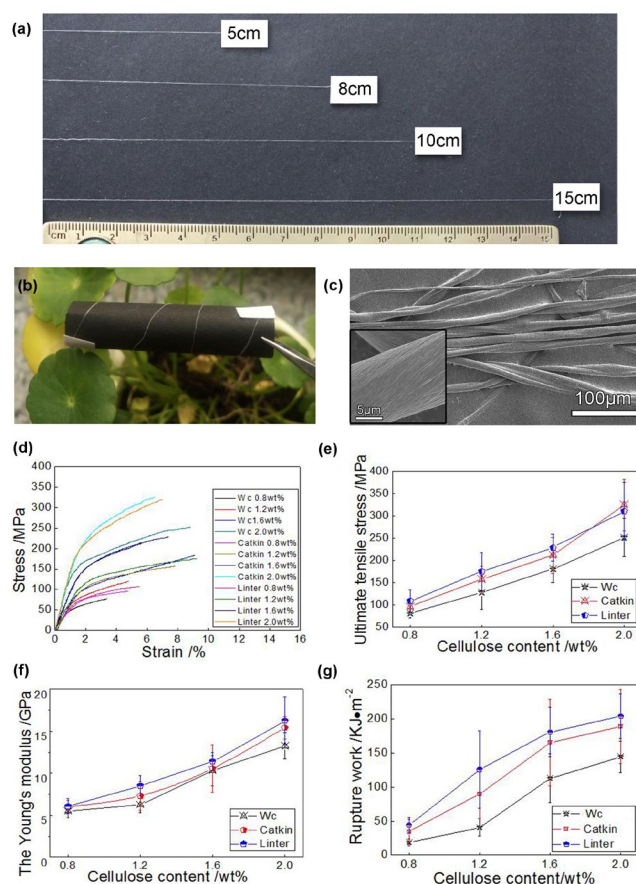


Figure 7: Photographs showing cellulose fibers with (a) controllable lengths and (b) good flexibility; (c) SEM images showing the micromorphological characteristics of the fibers; Mechanical properties of the fibers: (d) stress-strain curves, (e) UTS, (f) Young's modulus and (g) work of rupture

The cellulose/IL solutions prepared in the current study were also spun into long and flexible fibers using a needle syringe (Figs. 7(a) and 7(b)). The resulting fibers showed a spinal orientation and uniform thickness (Fig. 7(c)). The results of a mechanical tensile test on the fibers also revealed an elastic-plastic behavior, with remarkable increases in the UTS and Young's modulus values with increasing cellulose content (Fig. 7(d)). For example, increasing the cellulose content from 0.8 to 2.0 wt% led to an increase in the UTS from 77.84 to 330 MPa, as well as an increase in the Young's modulus from 5.48 to 16.27 GPa (Figs. 7(e) and 7(f)). The rupture work of cellulose fibers (regenerated from 2 wt% cellulose/IL) gave values of 144.63, 188.75 and 214.28 kJ/m² for the wood, catkin and linter samples, respectively (Fig. 7(g)). The UTS values of the regenerated cellulose fibers are above 200 MPa, which is greater than that of the fiber regenerated from pulp/TiO₂/[EMIM] Cl [30], highlighting the good durability and anti-fatigue properties of our regenerated fibers. These fibers could therefore be used as a reinforcing phase in composite materials, or as functional and smart materials (e.g., coating conductive materials of metal powders, carbon nanoparticles or conductive polymers).

4 Conclusion

High-purity [Bmim] Cl ionic liquid has been successfully prepared through the strategy of anhydrous calcium carbonate protection combined with the drop by drop reaction. The resulting [Bmim] Cl allowed for the rapid and complete dissolution of cellulose samples by heating under microwave irradiation. The regenerated cellulose materials mainly consisted of cellulose II crystals and displayed high DP and thermal stability properties. Cellulose films and fibers were prepared by properly reconstituting the cellulose chains during the regeneration process using the casting and injection methods, respectively. The cellulose resulting films possessed good flexibility and high light transmittance above 90%. The tensile strength and Young's modulus values of these films reached as high as 300 MPa and 14 GPa, respectively. The cellulose fibers exhibited good flexibility and mechanical properties with maximum ultimate tensile strength and Young's modulus values of 330 MPa and 16 GPa, respectively.

Acknowledgement: This work was supported by the National Natural Science Foundation of China (Grant No. 31800496) and Science Research Project Foundation of Shenyang University of Chemical Technology (No. LJ2019006).

Author contributions: D. Z. and X. W. designed the studies. X. W. performed most of the experiments. J. Z. and B. P. were involved in the analysis of mechanical data. D. Z. and X. W. co-wrote the paper. All authors commented on the manuscript.

Competing financial interests: The authors declare no competing financial interests.

References

1. Hassan, S. H., Voon, L. H., Velayutham, T. S., Zhai, L., Kim, H. C. et al. (2018). Review of cellulose smart material: biomass conversion process and progress on cellulose-based electroactive paper. *Journal of Renewable Materials*, 6(1), 1-25.
2. Zhao, D. W., Chen, C. J., Zhang, Q., Chen, W. S., Liu, S. X. et al. (2017). High performance, flexible, solid-state supercapacitors based on a renewable and biodegradable mesoporous cellulose membrane. *Advanced Energy Materials*, 7(18), 1700739.
3. Grande, R., Trovatti, E., Pimenta, M. T. B., Carvalho, A. J. (2018). Microfibrillated cellulose from sugarcane bagasse as a biorefinery product for ethanol production. *Journal of Renewable Materials*, 6(2), 195-202.
4. Chen, W. S., Zhang, Q., Uetani, K., Li, Q., Lu, P. et al. (2016). Sustainable carbon aerogels derived from nanofibrillated cellulose as high-performance absorption materials. *Advanced Materials Interfaces*, 3(10), 1600004.

5. Muthuraj, R., Sachan, A., Castro, M., Feller, J. F., Seantier, B. et al. (2018). Vapor and pressure sensors based on cellulose nanofibers and carbon nanotubes aerogel with thermoelectric properties. *Journal of Renewable Materials*, 6(3), 277-287.
6. Swatloski, R. P., Spear, S. K., Holbrey, J. D., Rogers, R. D. (2002). Dissolution of cellulose with ionic liquids. *Journal of the American Chemical Society*, 124(18), 4974-4975.
7. Zhao, H. B., Kwak, J. H., Wang, Y., Franz, J. A., White, J. M. et al. (2007). Interactions between cellulose and N-methylmorpholine-N-oxide. *Carbohydrate Polymers*, 67(1), 97-103.
8. Araki, J., Kataoka, T., Katsuyama, N., Teramoto, A., Ito, K. et al. (2006). A preliminary study for fiber spinning of mixed solutions of polyrotaxane and cellulose in a dimethylacetamide/lithium chloride (DMAc/LiCl) solvent system. *Polymer*, 47(25), 8241-8246.
9. Ramos, L. A., Frollini, E., Heinze, T. (2005). Carboxymethylation of cellulose in the new solvent dimethyl sulfoxide/tetrabutylammonium fluoride. *Carbohydrate Polymers*, 60(2), 259-267.
10. Sen, S., Martin, J. D., Argyropoulos, D. S. (2013). Review of cellulose non-derivatizing solvent interactions with emphasis on activity in inorganic molten salt hydrates. *ACS Sustainable Chemistry & Engineering*, 1(8), 858-870.
11. Cai, J., Zhang, L. N. (2005). Rapid dissolution of cellulose in LiOH/urea and NaOH/urea aqueous solutions. *Macromolecular Bioscience*, 5(6), 539-548.
12. Figoli, A., Marino, T., Simone, S., Di Nicolo, E., Li, X. M. et al. (2014). Towards non-toxic solvents for membrane preparation: a review. *Green Chemistry*, 16(9), 4034-4059.
13. Wang, H., Gurau, G., Rogers, R. D. (2012). Ionic liquid processing of cellulose. *Chemical Society Reviews*, 41(4), 1519-1537.
14. Kosan, B., Michels, C., Meister, F. (2008). Dissolution and forming of cellulose with ionic liquids. *Cellulose*, 15(1), 59-66.
15. Earle, M. J., Esperança, J. M., Gilea, M. A., Lopes, J. N. C., Rebelo, L. P. et al. (2006). The distillation and volatility of ionic liquids. *Nature*, 439(7078), 831-834.
16. Liu, B., Zhang, Z., Zhao, Z. K. (2013). Microwave-assisted catalytic conversion of cellulose into 5-hydroxymethylfurfural in ionic liquids. *Chemical Engineering Journal*, 215, 517-521.
17. Li, K., Kobayashi, T. (2016). A FT-IR spectroscopic study of ultrasound effect on aqueous imidazole based ionic liquids having different counter ions. *Ultrason Sonochem*, 28, 39-46.
18. Pathak, A. K., Ameta, C., Ameta, R., Punjabi, P. B. (2016). Microwave-assisted organic synthesis in ionic liquids. *Journal of Heterocyclic Chemistry*, 53(6), 1697-1705.
19. Zhang, L. N., Ruan, D., Gao, S. J. (2002). Dissolution and regeneration of cellulose in NaOH/thiourea aqueous solution. *Journal of Polymer Science Part B-Polymer Physics*, 40(14), 1521-1529.
20. Ahn, Y., Kwak, S. Y., Song, Y., Kim, H. (2016). Physical state of cellulose in BmimCl: dependence of molar mass on viscoelasticity and sol-gel transition. *Physical Chemistry Chemical Physics*, 18(3), 1460-1469.
21. Qi, H. S., Chang, C. Y., Zhang, L. N. (2009). Properties and applications of biodegradable transparent and photoluminescent cellulose films prepared via a green process. *Green Chemistry*, 11(2), 177-184.
22. Yano, H., Sasaki, S., Shams, M. I., Abe, K., Date, T. (2014). Wood pulp-based optically transparent film: a paradigm from nanofibers to nanostructured fibers. *Advanced Optical Materials*, 2(3), 231-234.
23. Zhang, X., Liu, X., Zheng, W., Zhu, J. (2012). Regenerated cellulose/grapheme nanocomposite films prepared in DMAc/LiCl solution. *Carbohydrate Polymers*, 88(1), 26-30.
24. Sundberg, J., Toriz, G., Gatenholm, P. (2015). Effect of xylan content on mechanical properties in regenerated cellulose/xylan blend films from ionic liquid. *Cellulose*, 22(3), 1943-1953.
25. Li, R., Zhang, L. N., Xu, M. (2012). Novel regenerated cellulose films prepared by coagulating with water: structure and properties. *Carbohydrate Polymers*, 87(1), 95-100.
26. Yang, Q. L., Fujisawa, S., Saito, T., Isogai, A. (2012). Improvement of mechanical and oxygen barrier properties of cellulose films by controlling drying conditions of regenerated cellulose hydrogels. *Cellulose*, 19(3), 695-703.
27. Klemm, D., Heublein, B., Fink, H. P., Bohn, A. (2005). Cellulose: fascinating biopolymer and sustainable raw material. *Angewandte Chemie International Edition*, 44(22), 3358-3393.

28. Li, Q., Chen, W. S., Li, Y. N., Guo, X. Y., Song, S. et al. (2016). Comparative study of the structure, mechanical and thermomechanical properties of cellulose nanopapers with different thickness. *Cellulose*, 23(2), 1375-1382.
29. Österberg, M., Vartiainen, J., Lucenius, J., Hippi, U., Seppälä, J. et al. (2013). A fast method to produce strong NFC films as a platform for barrier and functional materials. *ACS Applied Materials & Interfaces*, 5(11), 4640-4647.
30. Maxim, M. L., Sun, N., Swatloski, R. P., Rahman, M., Harland, A. G. et al. (2010). Properties of cellulose/TiO₂ fibers processed from ionic liquids. *ACS Symposium Series*, 14, 261-274.

Supporting Information

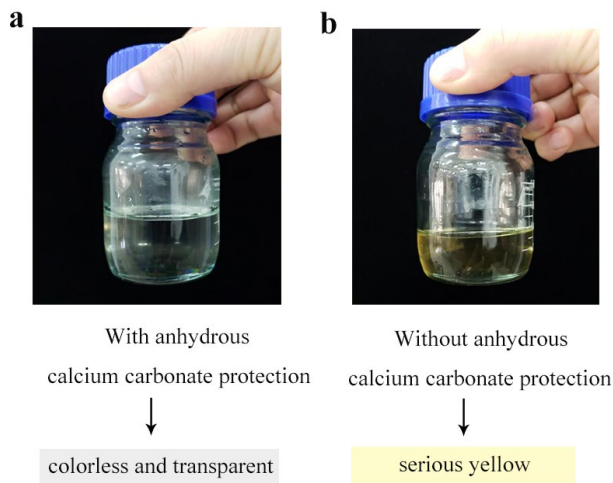


Figure S1: Optical images of the [Bmim] Cl prepared in the process of (a) calcium carbonate protection and (b) the absence of calcium carbonate protection

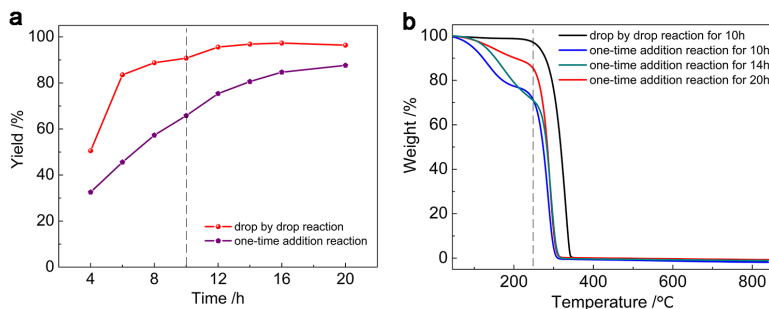


Figure S2: (a) Yield of the [Bmim]Cl as the function of the reaction time. (b) TG curves of the [Bmim] Cl prepared in the different reaction methods and time

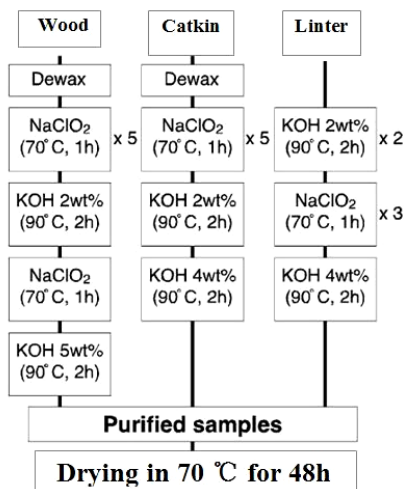


Figure S3: Experimental procedure for the preparation of cellulose samples from wood, catkin, and linter

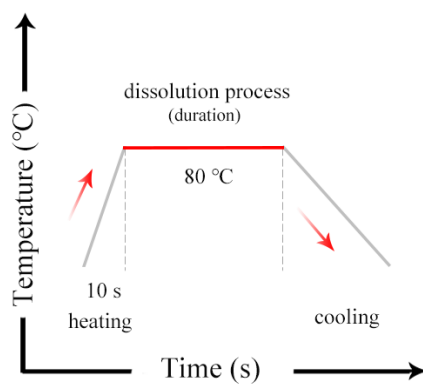


Figure S4: The temporal evolution of temperature during 1000 W thermal radiation

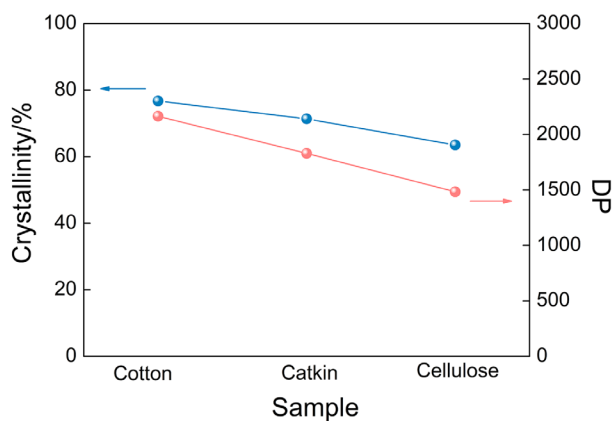


Figure S5: DP and crystallinity of cellulose from Wc, Catkin, and Linter

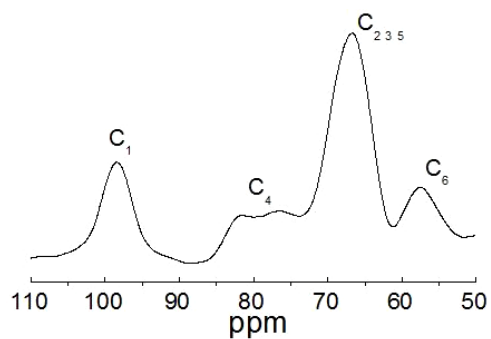


Figure S6: ^{13}C NMR spectrum of original cellulose

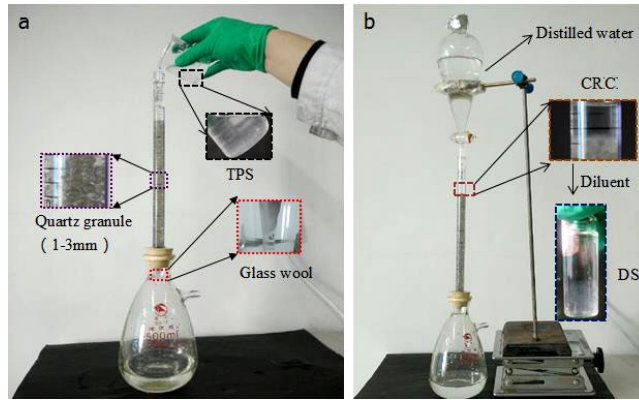


Figure S7: (a) The self-designed columnar filtration unit for the regeneration of dissolved cellulose samples; (b) washing the regenerated cellulose with distilled water

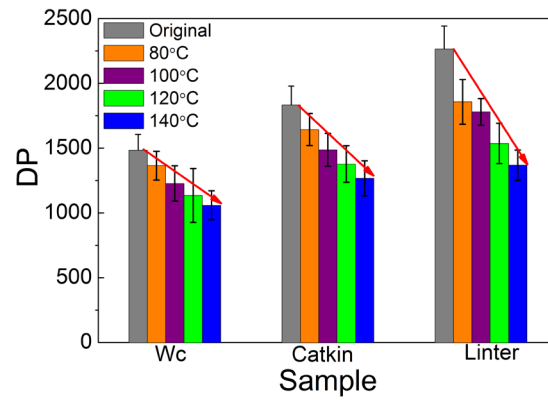


Figure S8: DP of cellulose from Wc, Catkin, and Linter depends on the solution temperature

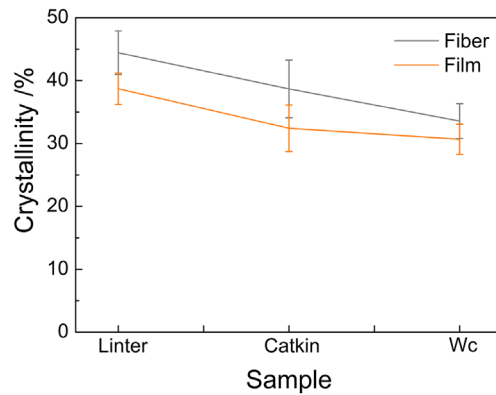


Figure S9: The crystallinity of cellulosic film and fiber regenerated from Wc, Catkin, and Linte

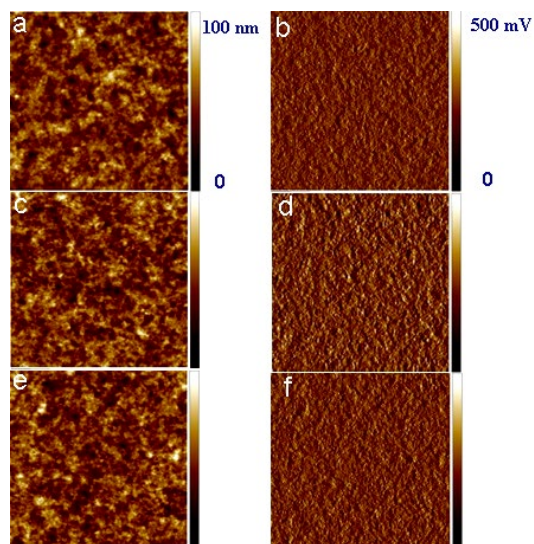


Figure S10: AFM micro-topographic (a, c, e) and phase (b, d, f) images of the regenerated cellulose films. (a, b) wood cellulose film. (c, d) catkin cellulose film. (e, f) linter cellulose film

Table S1: Chemical composition analysis of original and regenerated materials

| Sample | The percent of the three components | | |
|-------------|-------------------------------------|------------------|------------------|
| | a -Cellulose /% | Hemicellulose /% | Klason lignin /% |
| Wc | 89.21±0.72 | 10.14±0.26 | 0.56±0.12 |
| Linter-c | 96.33±0.38 | 3.14±0.07 | 0.31±0.08 |
| Catkin-c | 95.17±0.87 | 4.34±0.76 | 0.48±0.04 |
| RE Wc | 97.51±0.77 | 1.84±0.07 | 0.38±0.02 |
| RE Linter-c | 98.36±0.03 | 1.43±0.14 | 0.14±0.04 |
| RE Catkin-c | 98.55±0.06 | 1.49±0.09 | 0.11±0.03 |